LETTER • **OPEN ACCESS**

Imaging quantum dot formation in MoS_2 nanostructures

To cite this article: S Bhandari *et al* 2018 *Nanotechnology* **29** 42LT03

OPEN ACCESS
IOP Publishing

Letters
Nanotechnology

Nanotechnology **29** (2018) 42LT03 (5pp) https://doi.org/10.1088/1361-6528/aad79f

Letter

Imaging quantum dot formation in MoS_2 nanostructures

S Bhandari[1], K Wang[2], K Watanabe[3], T Taniguchi[3], P Kim[1] and R M Westervelt[1]

[1] School of Engineering and Applied Sciences and Department of Physics, Harvard University, MA 02138, United States of America
[2] School of Physics and Astronomy, University of Minnesota, MN 55455, United States of America
[3] National Institute for Materials Science, 1-1 Namiki, Tsukuba, 305-0044, Japan

E-mail: sbhandar@fas.harvard.edu

Received 21 May 2018, revised 26 June 2018
Accepted for publication 2 August 2018
Published 14 August 2018

Abstract

Among two-dimensional materials, semiconducting ultrathin sheets of MoS_2 are promising for nanoelectronics. We show how a scanning probe microscope (SPM) can be used to image the flow of electrons in a MoS_2 Hall bar sample at 4.2 K allowing us to understand device physics at the nanoscale. The SPM tip acts as a movable gate and capacitively couples the SPM tip to the device below. By measuring the change in device conductance as the tip is raster scanned across the sample, spatial maps of the device conductance can be obtained. We present images showing the characteristic 'bullseye' pattern of Coulomb blockade conductance rings around a quantum dot formed in a narrow contact as the carrier density is depleted with a backgate. These images show that multiple dots are created by the disorder potential in MoS_2. From these SPM images, we estimate the size and position of these quantum dots using a capacitive model.

Keywords: scanning probe microscope, MoS_2, quantum dots, imaging quantum dots

(Some figures may appear in colour only in the online journal)

1. Introduction

Ultrathin sheets of MoS_2, which are only a few atoms thick, conduct well and display electronic properties including a thickness- and strain-dependent bandstructure, valley Hall effects and spin-valley physics [1–6]. For graphene, covering both sides of a graphene sheet with layers of hexagonal boron nitride (hBN) greatly enhances the carrier mobility, resulting in ballistic transport [7]. However, the measured mobility in hBN-encapsulated MoS_2 devices is limited to moderate values (500–2000 $cm^2\,V^{-1}\,s^{-1}$) by scattering from lattice defects, charged impurities, and substrate adsorbates [8–15]. Direct imaging of electron motion in MoS_2 devices can give us vital information about device physics at the nanoscale, helping us to develop better devices. In previous research, we used our cooled SPM to image quantum dots formed in a GaAs 2DEG [16] and in an InAs/InP nanowire [17] by using the tip as a scanning gate to tune the number of electrons on the dot, creating rings of high conductance about the dot that correspond to Coulomb blockade conductance peaks [16, 17].

In this paper, we have adapted our SPM technique to image electron flow and characterize disorder in a MoS_2 device. We present conductance images that reveal quantum dot formation in a three layer MoS_2 device at 4.2 K, by using the tip to locally gate the quantum dot. The device is a hBN-MoS_2-hBN sandwich patterned into a Hall bar geometry, shown in figure 1(a). As the carrier density is reduced toward the charge neutral point, we find that quantum dots are created in the small side contact indicated in figure 1(a) by the

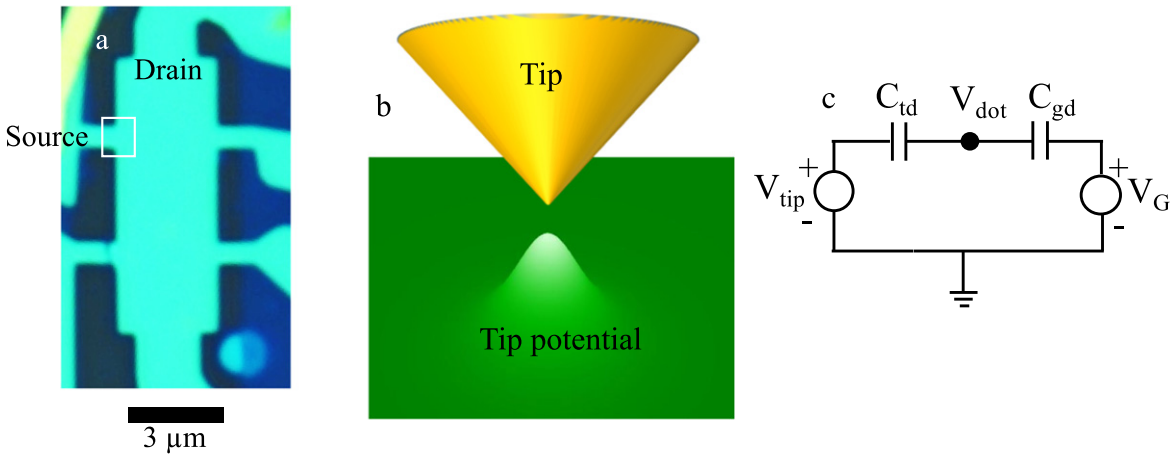

Figure 1. (a) Optical image of the hBN/MoS_2/hBN device patterned into (a) Hall bar geometry. The white outline indicates the region where SPM imaging experiments were performed. (b) Schematic diagram showing the potential inside the MoS_2 layer created by the SPM tip, which tunes the chemical potential of a quantum dot in the device below, changing the device conductance ΔG. An image is formed by displaying ΔG versus tip position as the tip is raster scanned across the sample. (c) Schematic circuit model of a quantum dot, showing the tip-to-dot capacitance C_{td} and the backgate-to-dot capacitance C_{gd} (see equation (3)).

white square, characterized by 'bullseye' pattern of Coulomb conductance peaks around each dot. From the spacing between the conductance rings and their dependence on backgate, we locate each dot and determine its radius.

2. Methods

2.1. Device fabrication

Using a dry transfer technique, we assembled a van der Waals heterostructure consisting of a few layer MoS_2 sheet contacting graphene sheets on all sides encased by two insulating hBN layers. The assembly is then transferred to a heavily doped silicon wafer covered with a SiO_2 layer that is 285 nm thick. The device is subsequently vacuum-annealed at 350 °C to reduce structural inhomogeneity. Finally, the Hall bar geometry is defined by reactive ion etching and a 1D edge contact to each graphene layer is fabricated with Cr/Pd/Au (1.5 nm/5 nm/120 nm) metal deposition.

Figure 1(a) shows an optical image of the Hall bar MoS_2 sample; the white square indicates the regions of image scans. The Hall bar is patterned from a hBN/MoS_2/hBN sandwich. It has dimensions 5.0 × 11.0 μm^2, with two narrow (1.0 μm) contacts along each side, separated by 3.0 μm, and large source and drain contacts (width 3.0 μm) at either end. The heavily doped Si substrate acts as a backgate, covered by a 285 nm insulating layer of SiO_2. The backgate capacitance is $C_G = 11.5$ nF. The density n can be tuned by applying a voltage V_G between the backgate and the MoS_2 channel. The density n is determined by hall measurements, using the side contacts.

2.2. Cooled scanning probe microscope (SPM)

We use a home-built cooled SPM to image quantum dot formation in our sample [16, 17]. The microscope assembly consists of a head assembly where the tip is attached and a cage assembly enclosing the piezotube translator that scans a sample fixed on top in the X, Y and Z directions. Scans are performed by actuating the piezotube with home-built electronics including an X–Y position controller for scanning, and a feedback Z controller for topological scans of the sample surface. The microscope assembly is placed in an insert inside a liquid He Dewar; the insert is filled with 3.0 mbar of He exchange gas to cool the sample and SPM. For the transport measurements, standard lock-in amplifiers are used. For the scanning gate measurements, an SPM tip of 10 nm radius was held at a fixed height 10 nm above the BN surface, which is approximately 50 nm above MoS_2 layer.

To image quantum dot formation using our cooled SPM, a voltage V_s is applied between a side contact and the grounded source of the device. At each tip position, the sample conductance $G = I_s/V_s$ is measured by the current I_s. The work function on the tip changes the chemical potential of a dot located inside the MoS_2 channel with a corresponding potential (figure 1(b)) that tunes the number of electrons in the dot, producing a change ΔG in the conductance. An image of rings of high conductance about the dot corresponding to Coulomb blockade conductance peaks is created by displaying ΔG as the tip is raster scanned above the sample at a constant height h.

2.3. Circuit model for tip-dot-backgate capacitance

Using a simple circuit model (figure 1(c)) we derive an expression to measure the radius of the quantum dot from the SPM images such as those shown in figure 4. The circuit includes the small tip-to-dot capacitance C_{td} and the large backgate-to-dot capacitance C_{gd} associated with the heavily doped Si substrate. The dot potential is V_{dot}, the backgate potential is V_G and the tip potential is V_{tip}. Using a standard model, the conical tip is modeled by two conducting spheres at the same potential: a small sphere with the tip radius a_{tip}

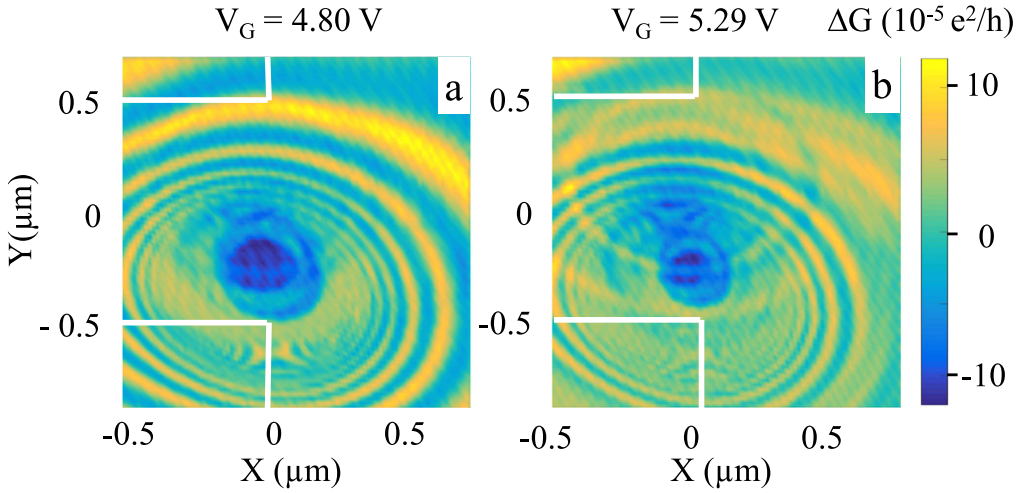

Figure 2. (a) Display of conductance change ΔG versus tip position at the narrow contact (see figure 1) for $V_G = 4.80$ V, when the device is nearly depleted. The bullseye pattern of concentric rings are Coulomb blockade conductance peaks associated with a quantum dot at the center. (b) As the density is increased for $V_G = 5.29$ V an additional quantum dot appears at a different location.

and a much larger sphere representing the top of the cone. When the tip is scanned across the sample, the distance is larger than the tip diameter, but generally small compared with the large sphere radius; the tip motion provides the contrast, while the top of the cone provides a background level. The tip-to-dot capacitance is given by:

$$C_{td} = \frac{4\pi\epsilon_o a_{dot} a_{tip}}{r_{td}}, \tag{1}$$

where a_{dot} is the dot radius, a_{tip} is the tip radius, and r_{td} is the distance between the tip and the dot. Similarly, the backgate-to-dot capacitance is given by:

$$C_{gd} = \frac{4\pi\epsilon_o a_{dot}^2}{2d}. \tag{2}$$

From the circuit model in figure 4(c), the dot charge q_{dot} is:

$$q_{dot} = (C_{td} V_{tip} + C_{gd} V_G). \tag{3}$$

We apply two methods to induce a change Δq_{dot} in the dot charge. Method 1 involves changing the tip position by Δr_{td} to induce a change in dot charge Δq_{dot} while keeping the backgate voltage V_G fixed. For this case

$$\Delta q_{dot} = \frac{dq_{dot}}{dr_{td}} \Delta r_{td} = \frac{dC_{td}}{dr_{td}} \Delta r_{td}. \tag{4}$$

Therefore, charge induced in the dot by a change in tip position Δr_{td} becomes

$$\Delta q_{dot} = (V_{tip} + V_G) \frac{4\pi\epsilon_o a_{dot} a_{tip}}{r_{td}^2} (\Delta r_{td}). \tag{5}$$

Method 2 involves inducing Δq_{dot} by a change in the backgate voltage V_G keeping the tip position fixed. For this method

$$\Delta q_{dot} = \frac{dq_{dot}}{dV_G} \Delta V_G = C_{gd} \Delta V_G. \tag{6}$$

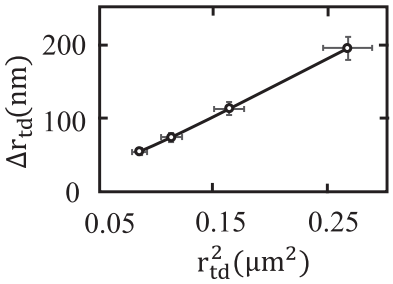

Figure 3. Spacing Δr_{td} between conductance rings versus radial distance r_{td} between the tip and bullseye center. The measured dot radius is $a_{dot} = 180$ nm.

3. Results and discussion

3.1. Experimental results

As the electron gas inside the MoS_2 device is depleted, the SPM images reveal the presence of quantum dots associated with pools of electrons at low points in the background potential. Figure 3(a) shows an image of ΔG taken inside the narrow contact at the upper left side (figure 1(a)). A clear bullseye pattern of Coulomb blockade conductance peaks circle the location of a quantum dot; the tip is acting as a movable gate, and the number of electrons on the dot changes by one as the tip moves from one ring to the next. As the electron density is increased in figure 2(b), a second quantum dot appears. Similar images of quantum dots were recorded previously for dots formed by top gates in a GaAs/AlGaAs heterostructure [16] and for an InAs dot formed in a InAs/InP nanowire [17].

3.2. Estimation of dot radius

Cooled SPM images of bullseye pattern of conductance rings are shown in figures 2(a) and (b). In these images, the backgate voltage is kept fixed at $V_G = 4.80$ V and $V_G = 5.29$ V,

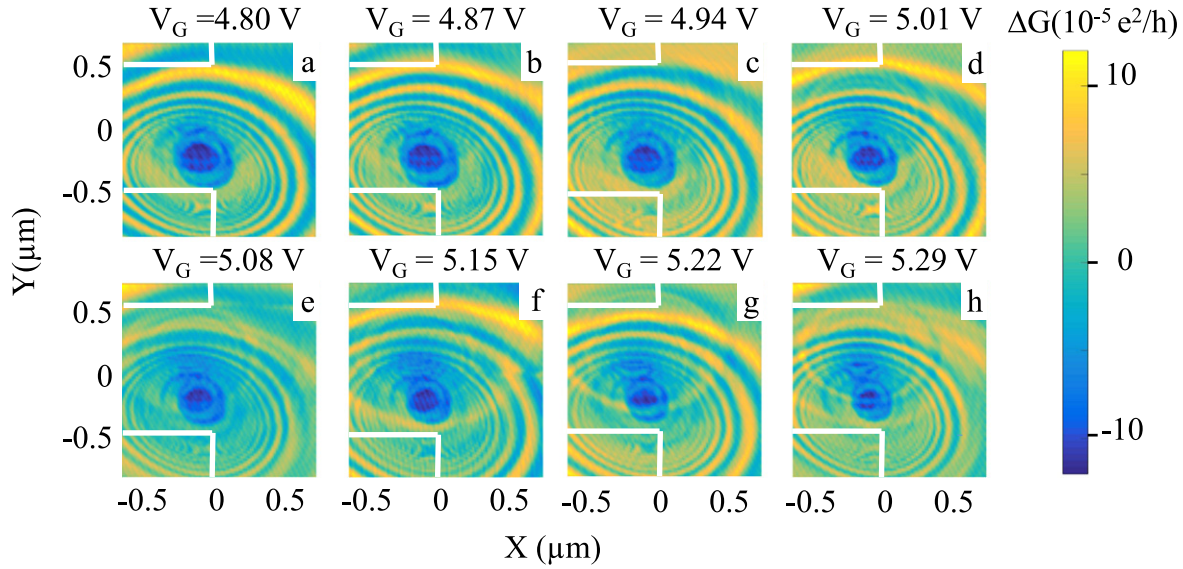

Figure 4. Images that display ΔG versus tip position in the narrow contact at the same locations as figure 3 for a series of backgate voltages indicated on the figure, ranging from (a) $V_G = 4.80$ V to (h) $V_G = 5.29$ V. The bullseye pattern of Coulomb conductance peaks in (a) shows the existence of a quantum dot. A second dot is created as V_G is increased.

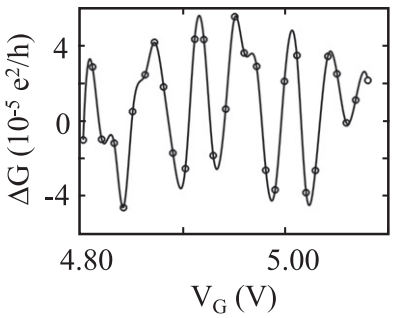

Figure 5. Plot of the conductance change ΔG from the series of images at tip position. $X = -0.5$ μm, $Y = 0.5$ μm versus V_G. To get the peak spacing, the peak position in V_G versus peak number is plotted and slope of this line gives average peak spacing $\Delta V_G = 50$ mV. Using the expression for charge induced in the quantum dot as V_G is varied, the measured dot radius is $a_{dot} = 150$ nm in good agreement with figure 4.

respectively. In figure 2(a), a single quantum dot is located at the center of the bullseye. Each conductance ring corresponds to an electron being added to the dot $\Delta q_{dot} = e$, where e is the electron charge, by changing the tip-to-dot capacitance via tip motion. Using Method 1, from the spacing between these rings and their distance from the center, we can compute the size and position of the dot. In figure 3, the plot of the ring spacing Δr_{td} versus r_{td}^2 shows a linear dependence which agrees well with equation (5). The slope determines the dot radius $a_{dot} = 180$ nm, using $V_{tip} = -1.00$ V and $a_{tip} = 10$ nm.

For Method 2, we keep the tip position fixed and change the backgate voltage V_G. figures 4(a)–(h) shows a series of SPM images of ΔG in the same location as figure 4 for backgate voltages ranging from (a) $V_G = 4.80$ V to (h) $V_G = 5.29$ V. An additional quantum dot appears as the density is increased.

To measure the effect of changing V_G, we pick a fixed tip position $X = -0.5$ μm, $Y = 0.5$ μm. Figure 5 plots ΔG at this tip position versus V_G. Figure 5 shows five peaks, and each peak corresponds to the addition of one electron charge e to the quantum dot. To get the peak spacing, the peak position in V_G versus the peak number is plotted. The slope of this line gives the average peak spacing $\Delta V_G = 50$ mV. By putting the average peak spacing in V_G into equation (6), we obtain the quantum dot radius $a_{dot} = 150$ nm, in good agreement with the dot radius found by Method 1.

4. Conclusion

In our imaging experiment, a cooled SPM shows quantum dots formation in the narrow side contacts in a MoS_2 Hall bar device at low electron density. We observe the characteristic bullseye pattern of Coulomb conductance peaks from two quantum dots formed in the narrow contact at the upper left of figure 1(a). Using a capacitive model, we estimate the dot radius using two methods to be $a_{dot} = 180$ nm and $a_{dot} = 150$ nm, in good agreement. The quantum dots are presumably formed by pools of electrons at minima in the background potential.

This paper demonstrates how a cooled SPM can image the presence of quantum dots created at low densities by roughness in the background potential, giving their location and radius, using our previously developed technique [16, 17]. By combining SPM imaging with photo-luminescence and Raman microscopy, investigators will be able to probe the sources of non-uniformity in MoS_2. This approach could be extended to sheets of other semiconducting transition metal dichalcogenide materials.

Acknowledgments

The SPM imaging experiments and the ray-tracing simulations were supported by the US DOE Office of Basic Energy Sciences, Materials Sciences and Engineering Division, under grant DE-FG02-07ER46422. The MoS_2 sample fabrication was supported by Air Force Office of Scientific Research contract FA9550-14-1-0268 and Army Research Office contract W911NF-14-1-0247. Growth of hexagonal boron nitride crystals was supported by the Elemental Strategy Initiative conducted by the MEXT, Japan and a Grant-in-Aid for Scientific Research on Innovative Areas No. 2506 'Science of Atomic Layers' from JSPS. Nanofabrication was performed in the Center for Nanoscale Systems (CNS) at Harvard University, a member of the National Nanotechnology Coordinated Infrastructure Network (NNCI), which is supported by the National Science Foundation under NSF award ECCS-1541959.

ORCID iDs

S Bhandari https://orcid.org/0000-0003-1007-9034
R M Westervelt https://orcid.org/0000-0001-9836-3923

References

[1] Kim S *et al* 2012 *Nat. Commun.* **3** 1011
[2] Mak K F, McGill K L, Park J and McEuen P L 2014 *Science* **344** 1489–92
[3] Mak K F *et al* 2012 *Nat. Nanotechnol.* **7** 494–8
[4] Conley H J *et al* 2013 *Nano Lett.* **13** 3626–30
[5] Han P *et al* 2018 *Nanotechnology* **29** 20
[6] Zhang Y *et al* 2012 *Nano Lett.* **12** 1136–40
[7] Dean C R *et al* 2010 *Nat. Nanotechnol.* **5** 722–6
[8] Xiao D, Liu G-B, Feng W, Xu X and Yao W 2012 *Phys. Rev. Lett.* **108** 196802
[9] Baugher B W, Churchill H O, Yang Y and Jarillo-Herrero P 2013 *Nano Lett.* **13** 4212–6
[10] Cui X *et al* 2015 *Nat. Nanotechnol.* **10** 6
[11] Oiu H, Pan L, Yao Z, Li J, Shi Y and Wang X 2012 *Appl. Phys. Lett.* **100** 123104
[12] Ayari A, Cobas E, Ogundadegbe O and Fuhrer M S 2007 *J. Appl. Phys.* **101** 014507
[13] Radisavljevic B and Kis A 2013 *Nat. Mater.* **12** 815–20
[14] Zhao P *et al* 2018 *2D Mater.* **5** 3
[15] Yan C *et al* 2018 *Nanotechnology* **29** 195704
[16] Fallahi P, Bleszynski A C, Westervelt R M, Huang J, Walls J D, Heller E J, Hanson M and Gossard A C 2007 *Nano Lett.* **5** 223–6
[17] Bleszynski A C, Froberg L E, Bjork M T, Trodahl H J, Samuelson L and Westervelt R M 2008 *Phys. Rev.* B **77** 245327